THE USE OF SPECTRAL METHODS IN PREDICTING THE REFLECTION AND TRANSMISSION OF ULTRASONIC SIGNALS THROUGH FLAWS

W. Dauksher
Boeing Commercial Airplane Group
P.O. Box 3707, MS 6H–CJ
Seattle, WA 98124

A. F. Emery
Department of Mechanical Engineering
Box 352600
University of Washington
Seattle, WA 98195–2600

INTRODUCTION

Finite difference solution of the wave equation will produce excellent results when the numerical procedure employs time increments and spatial discretization resulting in a Courant number of 1 for all elements. This ideal situation is difficult to achieve with reasonable mesh density when the modeling requires: 1) non–uniform grid discretization, 2) different materials or 3) more than one spatial dimension.

The development of a spectral finite element for solution of the wave equation is presented. Dispersive errors are quantified and compared to dispersive errors in finite difference models as a function of mesh density. Examples highlight the application of the developed spectral elements to multi–material systems with non–uniform mesh discretization.

DERIVATION OF THE FINITE ELEMENT EQUATIONS

The development of the spectral finite element equations is detailed. For a one dimensional member with constant geometry and material properties the governing equation is a hyperbolic partial differential equation. For u(x, t) and a wave velocity of c:

$$\frac{\delta^2 u}{\delta t^2} = c^2 \frac{\delta^2 u}{\delta x^2}. \tag{1}$$

On a finite interval the residual of equation (1) with an approximate solution is not necessarily equal to zero. The residual is multiplied by a weighting function, q, and the integral of the product is required to be zero.

$$\int_{\text{element}} q\left\{\frac{\delta^2 u}{\delta t^2} - c^2 \frac{\delta^2 u}{\delta x^2}\right\} dx = 0 \tag{2}$$

By limiting the weighting function q to only those functions which are zero at the extrema of the element, and integrating by parts:

$$\int_{\text{element}} \left\{q \frac{\delta^2 u}{\delta t^2} + c^2 \frac{\delta q}{\delta x} \frac{\delta u}{\delta x}\right\} dx = 0. \tag{3}$$

Review of Progress in Quantitative Nondestructive Evaluation, Vol. 15
Edited by D.O. Thompson and D.E. Chimenti, Plenum Press, New York, 1996

Following Patera [1], for an element of length L which lies on the interval [a, b] a local coordinate system is established:

$$\zeta = \frac{2}{L}(x-a)-1. \tag{4}$$

N+1 collocation points, ζ_i, are chosen in this local coordinate system:

$$\zeta_i = -\cos\frac{\pi i}{N} \qquad \text{where } i = 0, 1, 2, 3, ..., N. \tag{5}$$

The interpolant of $u(\zeta)$ for an element is written as:

$$u(\zeta) = \sum_{i=0}^{N} u_i h_i(\zeta) \tag{6}$$

where the u_i are the solution values at the collocation points. The h_i are Lagrangian interpolants which are zero outside the element, within the element satisfy $h_i(\zeta_j) = \delta_{ij}$ and are expressed as:

$$h_i(\zeta) = \frac{2}{N}\sum_{j=0}^{N}\frac{1}{c_i c_j} T_j(\zeta_j)T_j(\zeta) \tag{7}$$

where $c_n = 1$ for $0 < n < N$, $c_n = 2$ for $n = 0$, N and T_n are the Chebyshev polynomials defined as $T_n(x) = \cos(n \cos^{-1}(x))$.

The element's mass and stiffness matrices are obtained through integration of equation (3). A Galerkin form is used in which the weighting function q is the element shape functions h_i. M^e_{ij} and K^e_{ij} are the i^{th} row and j^{th} column components of the element's mass and stiffness matrices. The matrices are symmetric.

$$M^e_{ij} = \int_{\text{element}} h_i h_j dx = \frac{2L}{N^2 c_i c_j}\sum_{m=0}^{N}\sum_{n=0}^{N}\frac{1}{c_m c_n} T_m(\zeta_i)T_n(\zeta_j)\int_{-1}^{1} T_m T_n dx \tag{8}$$

$$K^e_{ij} = \int_{\text{element}} \frac{dh_i}{dx}\frac{dh_j}{dx} dx = \frac{8}{LN^2 c_i c_j}\sum_{m=0}^{N}\sum_{n=0}^{N}\frac{1}{c_m c_n} T_m(\zeta_i)T_n(\zeta_j)\int_{-1}^{1} \frac{dT_m}{dx}\frac{dT_n}{dx} dx \tag{9}$$

Following Zienkiewicz [2], the temporal finite element formulation assumes a form:

$$\begin{aligned}\left(M^g + \beta\Delta t^2 K^g\right)u^{t+\Delta t} + \left(-2M^g + (1/2-2\beta+\alpha)\Delta t^2 K^g\right)u^t \\ + \left(M^g + (1/2+\beta-\alpha)\Delta t^2 K^g\right)u^{t-\Delta t} = 0\end{aligned} \tag{10}$$

with α and β as weighting functions in the temporal integration. M^g and K^g are the system's global mass and stiffness matrices and u is a column matrix of the unknown nodal displacements. The choice of α and β govern the recurrence scheme employed. Forward marching solutions are based on solutions at the two previous time steps, t and $t-\Delta t$, permitting evaluation at the future time step, $t+\Delta t$.

The temporal weighting functions are chosen as $\beta=0$ and $\alpha=1/2$ which results in the central difference approach. This simplification places stability limits on the maximum permissible time increment Δt. Equation (10) simplifies to:

$$M^g u^{t+\Delta t} + \left(-2M^g + \Delta t^2 K^g\right)u^t + M^g u^{t-\Delta t} = 0. \tag{11}$$

The mass matrix, M^g, is populated by terms from equation (8). To avoid the cost associated with using an inverted (fully populated) consistent mass matrix to solve for u in equation (11), a method henceforth called row summing is employed. In row summing all masses on a given row in the mass matrix are added to that row's diagonal term. All non–

diagonal terms are then set to zero. The system's mass is conserved. All further applications presented will be for a row summed mass matrix in equation (11).

ACCURACY – DISPERSION IN THE SPECTRAL METHOD

Piece–wise continuous modeling of a continuous isotropic medium will generate numerically dispersive and anisotropic solutions [3]. To numerically evaluate the dispersive errors, a displacement field is imposed on the mesh with the form:

$$u = Av\exp(i\omega t) \quad \text{where} \quad A_i = A(x_i) \quad \text{and} \quad v_i = \cos(\gamma x_i) \tag{12}$$

where A(x) is the amplitude of the imposed displacement field, ω is the radial frequency, $v(x, \gamma)$ is a spatially varying function and γ is the wavenumber.

In a dispersive medium, waves of different frequencies will travel at different velocities [4]. The phase velocity, c_{po}, is equivalent to ω/γ where $\omega(\gamma)$ and is not necessarily equal to the true velocity c_o. Similarly, the group velocity, c_{gr}, is defined as $d\omega/d\gamma$ and is not necessarily equal to c_o. The numerical solution for $\omega(\gamma)$ is obtained by finding the roots of the system of equations:

$$\left\{M^g \exp(i\omega\Delta t) + \left(-2M^g + \Delta t^2 K^g\right) + M^g\exp(-i\omega\Delta t)\right\}Av\exp(i\omega t) = 0. \tag{13}$$

For an isotropic infinite medium, the amplitude of the wave field, A, becomes a constant A_o. Noting that the imaginary components of $\exp(i\omega\Delta t)$ and $\exp(-i\omega\Delta t)$ cancel, the resulting system of equations takes the form:

$$A_o\left\{2M^g\cos(\omega\Delta t) + \left(-2M^g + \Delta t^2 K^g\right)\right\}v\exp(i\omega t) = 0. \tag{14}$$

Equation (14) may be treated as an eigenvalue problem with A_o and $\exp(i\omega t)$ considered nonzero for the non–trivial solution. The $\cos(\omega\Delta t)$ terms are the eigenvalues and the v are the corresponding eigenvectors.

$$\left[M^g - \frac{1}{2}\Delta t^2 K^g\right]v = \cos(\omega\Delta t)[M^g]v \tag{15}$$

For each ω found in equation (15), the corresponding wavenumber, γ, is found iteratively. A least squares error procedure calculates the appropriate value γ from the eigenvector v. The resulting fit is considered acceptable for an average error per data point of less than 0.1%.

Phase and group velocity errors can be quantified by examining dispersion curves. Values of ω and γ are used to obtain c_{po} and c_{gr} vs c_o as shown in figure 1. The spectral element considered is of 6^{th} order. The disparity in accuracy between the linear finite difference and any of the spectral elements would have resulted in all spectral element curves clustered on top of one another. 6^{th} order was chosen as representative of the spectral method's accuracy. In figure 1, τ is the ratio of time step taken to the maximum permissible (stable) time step and G is the average number of nodes per wavelength. For the linear finite difference data, τ is equivalent to the Courant number. The results for linear finite difference match those published by Marfurt [3]. For the row summed mass matrix case the following general conclusions are drawn:

1) increase in mesh density decreases dispersion.
2) group velocity dispersion is more significant than phase velocity dispersion.
3) as expected for τ=1, linear finite difference offers no dispersion.
4) for other values of τ, the spectral method produces significantly less dispersion.

The effect of spectral element order on dispersion is detailed in figure 2 for the row summed mass matrix. The 'bumpy' nature of the row summed curves is a manifestation of the numerical solution for wavelength and the minute dispersion this method offers. These results were generated at a τ of 1. Significant conclusions drawn from figure 2 include:

1) group velocity dispersion is greater then phase velocity dispersion.
2) increase in element order results in a decrease in dispersion.

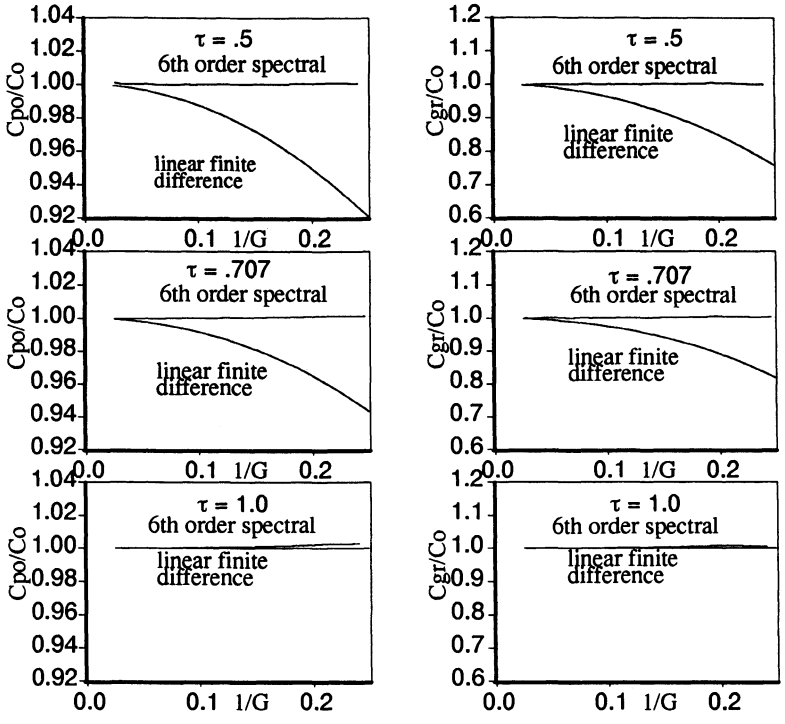

Figure 1 – Dispersion in row summed mass matrix solutions to the one dimensional wave equation for linear finite elements and 6th order spectral elements. For the one dimensional case, row summed linear finite elements are equivalent to linear finite difference elements. The average number of nodes per wavelength is taken as G. τ is the ratio of time step used to the maximum stable time step.

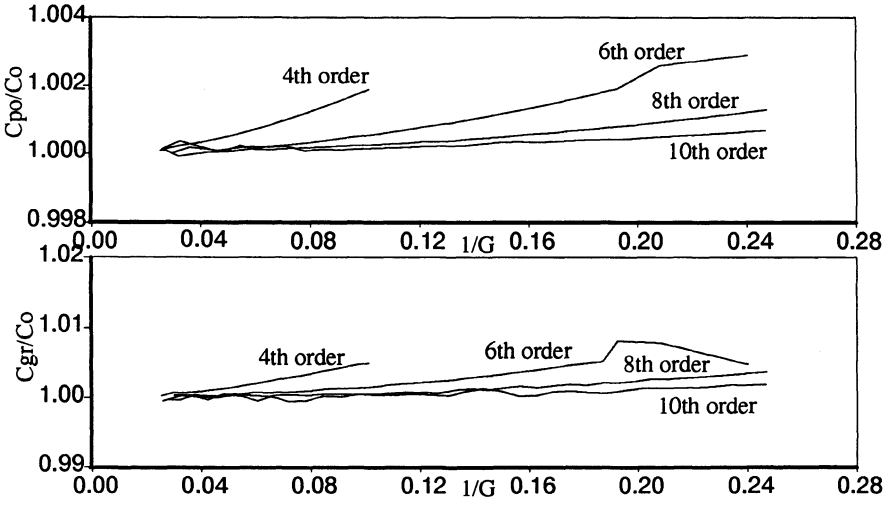

Figure 2 – Comparison of group and phase velocity errors for row summed mass matrix spectral elements as a function of element order.

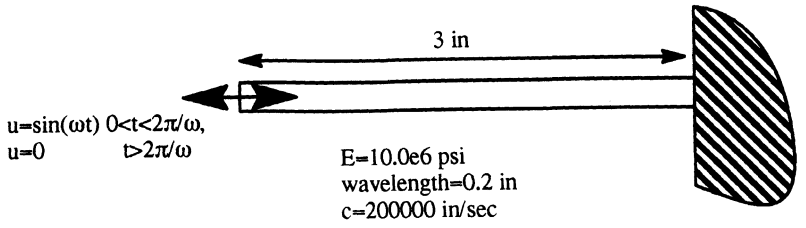

Figure 3 – Rod subject to single sinusoidal impulse.

EXAMPLES

A simple rod model was used to evaluate the practical application of the spectral method to the 1D wave equation. For all examples the mass matrices are row summed and the prior choice of $\beta=0$ and $\alpha=1/2$ in the temporal discretization is enforced. The system is shown in figure 3. A single sinusoidal pulse is applied to the end of an aluminum rod which is fixed at the far end. Figure 4 a) presents the solution at 13 μsec as modeled with 11^{th} order spectral elements with a mesh density of 20 nodes per wavelength.

For comparison, linear finite difference modeling of the same event results in the response shown in figure 4 b). The finite difference model uses the same time step, Δt, as the above described spectral run which corresponds to $\tau=.18$ for the finite difference procedure. Results in this case are poor and demonstrate the errors induced by the finite difference approach with a Courant number of significantly less than 1. The dispersive nature of finite difference solutions to the wave equation at Courant numbers less then 1 is well documented [3, 5, 6, 7, 8, 9].

The fidelity of spectral element method solutions of acoustic wave problems with inclusions is studied by examining the responses of the system pictured in figure 5. Fourteen 21^{st} order spectral elements evenly discretize material 1. Material 2, the inclusion, is modeled as a single element with a mesh density of slightly >18 nodes per wavelength. The studied inclusion thicknesses are .1 in, .01 in and .001 in.

Figures 6 depicts system response at 13μsec for the studied inclusion thicknesses. Observations include:

1) the effect of inclusion thickness and wave velocity are evident in comparing figures 6 a), b) and c). In 6 b) the inclusion is thin enough that the reflection off the far side of the inclusion reflects back to positively amplify the trough of the initial reflection. In 6 a) the inclusion thickness and wave speed are such that this positive interference does not occur; two distinct reflected waves are evident.
2) the magnitude and shape of the reflected waves are markedly different between figure 6 b) and c). Intuitively, the .001 in inclusion is so thin that its axial stiffness, AE/L, could cause it to respond more like a rigid link between the two more flexible materials 1.

The exercise detailed in figure 6 indicates that reflected waves which could be used to characterize an inclusion may be accurately modeled with the spectral element method developed. Reflected wave amplitude and shape indicate inclusion's thickness and wave–speed. A pressure transducer would monitor stresses and, hence, the nature of reflected waves. Typical stresses measured at the input surface for the three inclusions studied are presented in figure 7. Comparison of the wave motion snapshots of figure 6 with the stresses of figure 7 gives a physical intuition to the recorded stress histories.

The finial 1D model study involves a gap replacing the inclusion (figure 8). The gap is modeled as a 2^{nd} order element with a bi–linear Young's modulus. In compression the gap possesses the stiffness of the adjacent material. In tension, the extensional stiffness of the gap is taken as 1/10 that of the adjacent material. Numerical restrictions prohibited the total degradation of the gap's tensile modulus. Materials 1 were modeled with 21^{st} order elements and evenly discretized at slightly >20 nodes/wavelength. The solution technique involved the use of 2 stiffness matrices, one for a closed gap and one for an open gap. When the gap switched from open to closed, or closed to open, the temporal iteration was run to a

point as close to an unloaded gap stress state as possible. Stiffness matrices were then switched. This procedure minimized errors induced by predicting displacements in a gap (open/closed) state with the improper (closed/open) stiffness matrix. Figure 9 depicts the displacement waves at three instances. In 9 b) the splitting of the initial incident wave due to gap opening is evident. Figure 10 presents the stress history as measured close to the surface and gap opening displacements.

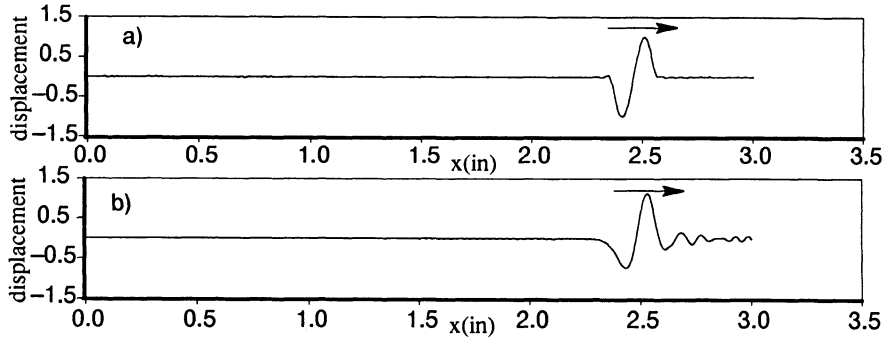

Figure 4 – Wave prior to incidence with end; arrow indicates direction of travel. a) spectral 11th order elements at 20 nodes per wavelength, b) finite difference solution run at same time step (Courant number of .1854) and 20 nodes per wavelength.

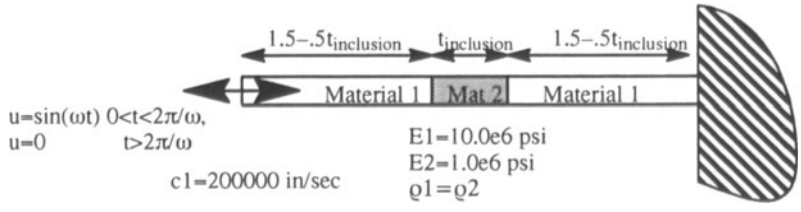

Figure 5 – Rod with central inclusion.

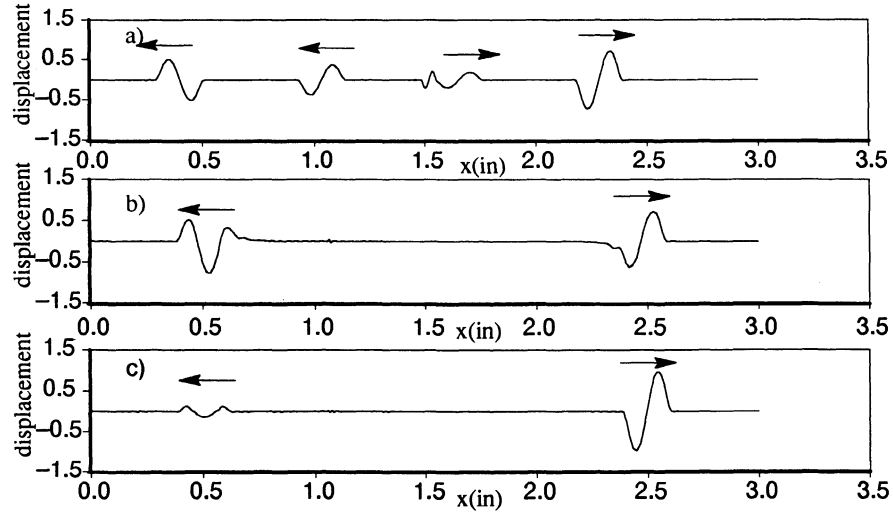

Figure 6 – Wave motion in the rod with inclusion at 13 μsec. Inclusion thicknesses of: a) .1 in, b) .01 in and c) .001. Initial wave incidence on inclusion at ~7.5 μsec.

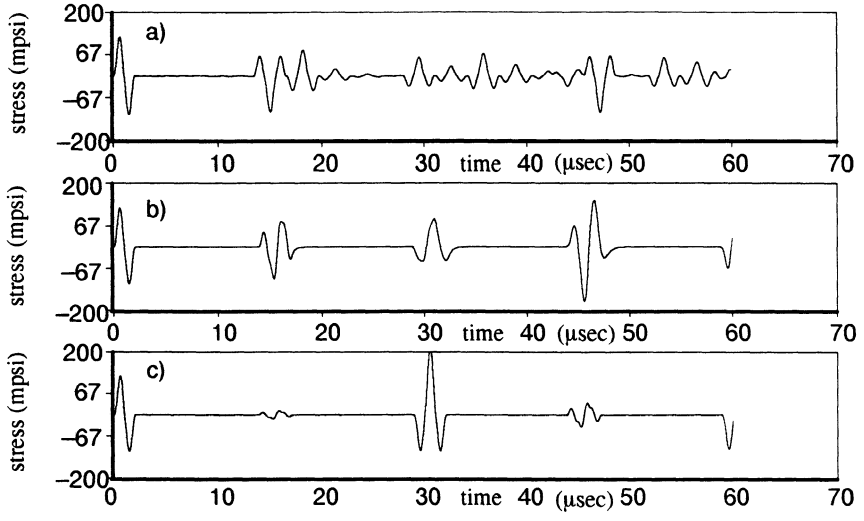

Figure 7 – Stresses measured by sensor at the input surface of rod with inclusion. Inclusion thicknesses are: a) .1 in, b) .01 in, and c) .001 in.

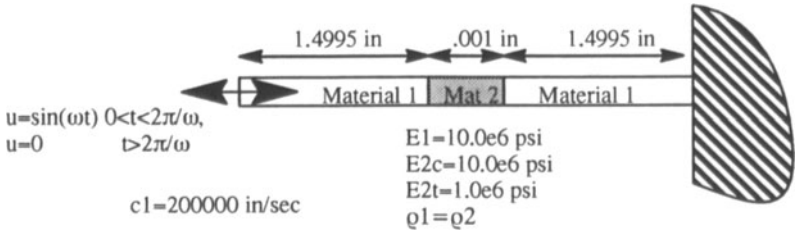

Figure 8 – Rod with gap modeled as bi–linear material subject to single sinusoidal impulse.

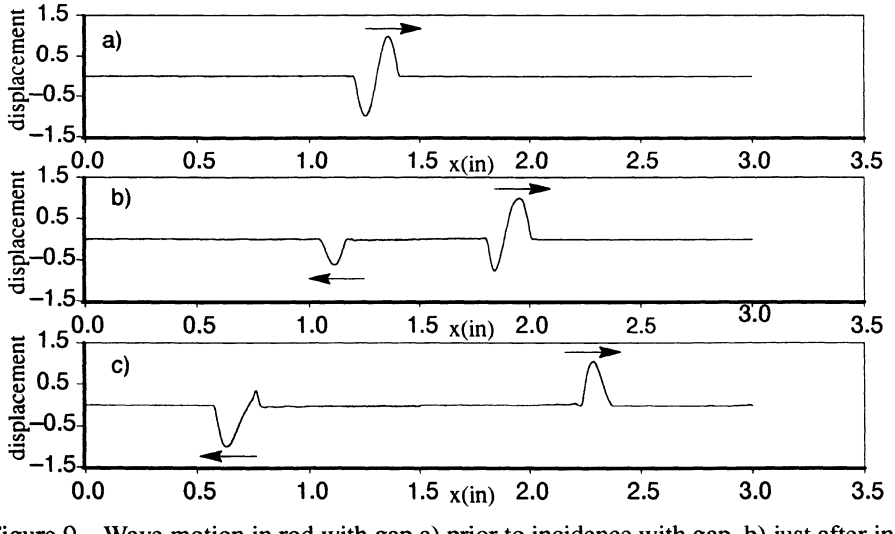

Figure 9 – Wave motion in rod with gap a) prior to incidence with gap, b) just after incidence with gap and c) after second incidence with gap.

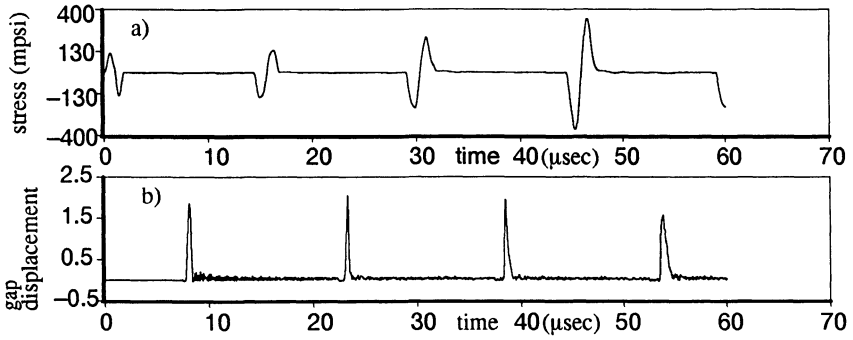

Figure 10 – a) stresses measured just below the surface of the input end of the gap model and b) gap displacement (+ opening).

CONCLUSIONS

Row summed spectral finite elements with a central difference time discretization can be used to solve the 1D wave equation. This alleviates the cost of a solution with an inverted (fully populated) mass matrix.

Dispersive errors in spectral finite element solutions to the 1D wave equation employing a central difference time scheme and row summing have been shown to be significantly less than those for finite difference solutions at Courant numbers <1. Additionally, an increase in spectral element order has shown to markedly decrease dispersive errors.

The ability of these spectral finite elements to predict the surface signatures (i.e. stresses) of internal defects has been demonstrated.

REFERENCES

1. Patera, A. T., 1984, A Spectral Method for Fluid Dynamics: Laminar Flow in a Channel Expansion, Journal of Computational Physics, 54, 468–488.
2. Zienkiewicz, O. C., 1977, *The Finite Element Method*, 3rd edition, McGraw Hill, London.
3. Marfurt, K. J., 1984, Accuracy of Finite Difference and Finite Element Modeling of the Scalar and Elastic Wave Equations, Geophysics, 49, no 5, 533–549.
4. Brillouin, L., 1953, *Wave Propagation in Periodic Structures*, 2nd edition, Dover, New York.
5. Canuto, C., Hussaini, M. Y., Quarteroni, A., and Zang, T. A., 1988, *Spectral Methods in Fluid Dynamics*, Springer–Verlag, Berlin.
6. Dablain, M. A., 1986, The Application of Higher Order Differencing to the Scalar Wave Equation, Geophysics, 51, 54–66.
7. Emery, A. F., The Use of Finite Element Methodology in Designing Ultrasonic Tests and the Detection of Weak Bond Planes, unpublished report to Sandia National Laboratory.
8. Trefethen, L. N., 1982, Group Velocity and Finite Difference Schemes, SIAM Review, 24, 113–136.
9. Alford, R. M., Kelly, K. R., and Boore, D. M., 1974, Accuracy of Finite Difference Modeling of the Acoustic Wave Equation, Geophysics, 39, 834–842.